Sensitivity of Simulated Steel Column Instabilities to Plasticity Model Assumptions

Alexander Hartloper[1], Albano de Castro e Sousa[2], Dimitrios G. Lignos[3]

[1] Doctoral Assistant, Faculté de l'Environnement Naturel, Architectural et Construit (ENAC), École Polytechnique Fédérale de Lausanne (EPFL), Suisse.

[2] Postdoctoral Researcher, Faculté de l'Environnement Naturel, Architectural et Construit (ENAC), École Polytechnique Fédérale de Lausanne (EPFL), Suisse.

[3] Associate Professor, Faculté de l'Environnement Naturel, Architectural et Construit (ENAC), École Polytechnique Fédérale de Lausanne (EPFL), Suisse.

ABSTRACT

Current experimental studies on the seismic behavior of steel wide-flange columns under multi-axis cyclic loading reveal that these members, depending on their geometric characteristics, may be susceptible to axial shortening, out-of-plane deformations and lateral-torsional buckling coupled with local buckling. In that respect, simulation models have intrinsic value to generalize the previous experimental findings in a wider range of member sizes and aid the further development of our seismic design and assessment standards. Prior work on continuum finite element (CFE) modeling of steel wide-flange columns stressed the importance of the proper consideration of local and member imperfections within the CFE model. The assumptions underlying the steel material model, particularly its hardening laws, along with the methodology for obtaining its input parameters, have been overlooked. The main issue explored in this paper centers on the fact that commonly used nonlinear isotropic/kinematic plasticity models within CFE simulation platforms were originally developed for stainless steels. Therefore, they do not represent the discontinuous yielding phenomenon present in typical structural mild steels. Nonlinear analyses conducted in this paper underscores that the predicted buckling modes are sensitive to the choice of material model for a class of steel wide-flange columns.

Keywords: material model, modeling recommendations, instabilities, steel columns, multi-axis plasticity.

INTRODUCTION

A number of experiments have been carried out in the past decade to better characterize the behavior of steel wide-flange columns under multi-axis cyclic loading [1-6]. These experiments suggest that coupled local buckling and lateral-torsional buckling (LTB) in columns is likely to occur, followed by axial shortening, and out-of-plane deformations. As highlighted by these experiments, the aforementioned instability modes are dependent on a column's local and member slenderness characteristics, boundary conditions, axial load, and the imposed lateral loading sequence.

While physical experiments are essential to characterize column behavior, they are limited by the number of cross-sections, column lengths, boundary conditions, lateral load patterns, and axial load demands can be reasonably tested. Continuum finite element (CFE) simulations are valuable in this regard to extend the findings from these experiments to a wider range of these variables. For example, CFE parametric studies have been used to evaluate design guidelines [7], propose updates to current standards [8] and to improve nonlinear modeling recommendations [9]. Chiefly, CFE analyses on columns are sensitive to the geometric imperfections chosen to realistically model geometric instabilities, and the material model chosen to represent the nonlinear behavior of the steel material. While prior studies have focused on calibration of the local and member imperfections required to capture observed instability modes [8, 10], the use of classic metal plasticity models has been taken for granted.

At present, the nonlinear cyclic behavior of metals is typically modeled through a combined isotropic and kinematic hardening approach based on the work of Voce [11] and Chaboche et al. [12], respectively (the latter being an extension of the work done by Armstrong and Frederick [13]). Despite the pervasive use of this model in CFE software packages, unbiased calibrations based on cyclic uniaxial experiments reveal its inherent deficiencies in capturing the discontinuous yielding phenomenon present in mild steels. This paper introduces the issues with this classic plasticity model for mild steels, and how they can be addressed. Furthermore, CFE simulations illustrate that modeling of the discontinuous yielding phenomenon can have a significant impact on the predicted buckling modes of steel wide-flange columns under multi-axis cyclic loading.

UPDATED MATERIAL MODEL

Modeling the discontinuous yielding phenomenon

The discontinuous yielding phenomenon in mild steels is widely accepted to be the result of dislocation locking within the steel microstructure due to interstitial carbon and nitrogen solute atoms [14-16]. A stress-strain relationship for a mild steel is shown schematically in Figure 1a. Here, key characteristics of materials with discontinuous yielding can be seen, notably: the upper yield stress ($\sigma_{y,u}$), the yield plateau and associated lower yield stress, $\sigma_{y,0}$, followed by strain hardening within the material. The plateau region in these materials is associated with the stripping of dislocations from their carbon and nitrogen atmospheres, and discontinuous yielding is not present after this region upon immediate reloading at room temperatures.

Cyclic tension-compression tests on mild steel coupons reveal that the yield stress is diminished below the lower yield stress after the first inelastic loading excursion (i.e., once dislocations have been stripped from their atmospheres). This observation is shown schematically in Figure 1a, where twice the initial yield stress (assumed equal with the lower yield stress), $2\,\sigma_{y,0}$ is greater than twice the yield stress upon immediate reloading, $2\,\sigma_y^{(1)}$. The yield stress evolution in terms of the equivalent plastic strain, ε_{eq}^p, is shown schematically in Figure 1b. The equivalent plastic strain represents the total accumulated plastic strain that a material infinitesimal point has experienced and is typically used as an internal variable in metal plasticity constitutive models. Figure 1b illustrates that there is a reduction in the size of the yield surface after some amount of plastic straining. Figure 1b also shows that at a particular equivalent plastic strain, denoted by ε_r, the size of the yield surface is recovered due to cyclic hardening. However, whether the initial yield stress is recovered may depend on the material; thus, the relation requires further testing to be quantified.

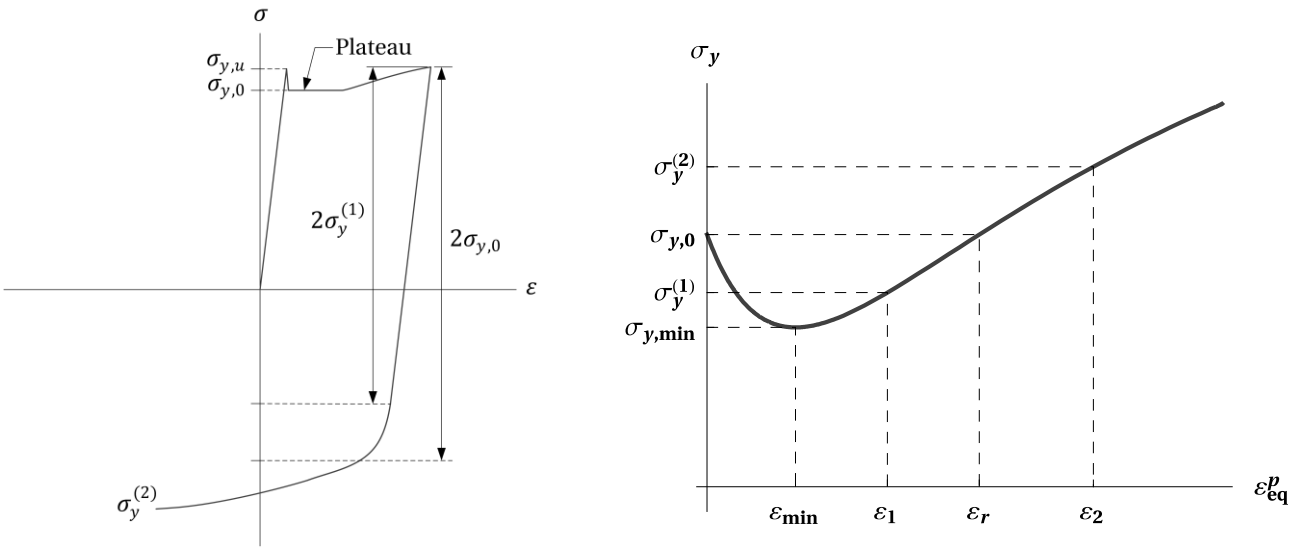

(a) Stress-strain *(b) Evolution of the yield stress*

Figure 1. Schematic illustrations of a mild steel's response under cyclic loading.

The mathematical representation of mild steels is now discussed. This model employs a von Mises yield criterion with combined nonlinear isotropic and kinematic hardening. The isotropic hardening rule controls the size of the yield surface, σ_y. Voce [11] proposed the isotropic hardening rule given in Eq. (1),

$$\sigma_y = \sigma_{y,0} + Q_\infty\left(1 - exp\left[-b\,\varepsilon_{eq}^p\right]\right), \tag{1}$$

where Q_∞ defines the maximum increase in yield stress due to hardening at saturation (saturation occurs as $\varepsilon_{eq}^p \to \infty$), and b defines how quickly this term approaches saturation. Isotropic hardening defined by Eq. (1) increases monotonically with increasing equivalent plastic strain. Therefore, it is not possible to approximate the curve shown in Figure 1b. When the Voce isotropic hardening rule is used to model mild steel subjected to cyclic loading, this incompatibility manifests itself by either underestimating the initial yield stress, or by overestimating the yield stress in subsequent plastic loading excursions. Both these issues can be attributed to the fact that the there is a permanent decrease in the yield stress not accounted for in the Bauschinger effect [17]. If several plastic loading cycles are employed to calibrate the material parameters, then a better fit is obtained by typically reducing the initial yield stress than overpredicting the yield stress in each cycle. Hence, the error is

primarily focused in the first loading cycle as opposed to every cycle thereafter. Preliminary results suggest that this underestimation of the initial yield stress can be on the order of 10-20 % [18].

A new isotropic hardening rule is proposed to alleviate the aforementioned issues. A summation of two isotropic hardening components is proposed similar to Chaboche et al. [12]. However, the key difference is that the second component has the effect of diminishing the yield surface. The updated isotropic rule is provided in Eq. (2),

$$\sigma_y = \sigma_{y,0} + Q_\infty\left(1 - exp\left[-b\ \varepsilon_{eq}^p\right]\right) - D_\infty\left(1 - exp\left[-a\ \varepsilon_{eq}^p\right]\right), \tag{2}$$

where D_∞ and a are parameters of the same nature as Q_∞ and b. If $D_\infty = 0$, the proposed model reduces to the original material model. Eq. (2) is used to represent the behavior shown in Figure 1b, while the combination of isotropic and kinematic hardening provides the full behavior of the material. The additional term is novel in its purpose to model the discontinuous yielding phenomenon as it can account for the permanent decrease in the yield stress observed in cyclic tests on mild steels [17]. Explicitly, the purpose of implementing the updated material isotropic hardening rule is to increase the initial yield stress compared to the original model, and to provide an initial plateau in the stress-strain response.

Finally, the kinematic hardening rule used to control the location of the center of the yield surface in stress space in the updated material model is the same as that in Chaboche et al. [12], and therefore is only briefly discussed. Chaboche et al. [12] proposed to take the summation of several backstress terms defined by the Armstrong-Frederick rule [13]. Each backstress term is defined by C_k that is related to the increase in stress due to kinematic hardening at saturation for backstress k, and the corresponding rate term, γ_k.

Model implementation

The updated Voce-Chaboche material model outlined in the previous section is implemented as a UMAT user subroutine in the Abaqus version 6.14 [19] simulation platform for uniaxial, plane-stress, and multiaxial stress states so to be compatible with a wide range of elements. The UMAT files are publicly available at https://resslab.epfl.ch/RESSLab-tools. Each of the implementations are validated with the built-in nonlinear isotropic/kinematic material model in Abaqus by using the same parameters for both models (i.e., the updates are ignored for the validation, $D_\infty = 0$, $a \neq 0$). Figure 2a and 2b show the true stress – strain relationships from the same integration point of a single element, where "Abaqus" uses the built-in commercial model, and "UMAT" uses the implemented UMAT. A single four-node shell element (S4) is subjected to a biaxial stress state in the plane-stress case, while a single 8-node solid (C3D8) element is subjected to a biaxial stress state for the multiaxial case. From the two figures, the UMAT agrees with the built-in material model for both cases to the order of machine precision.

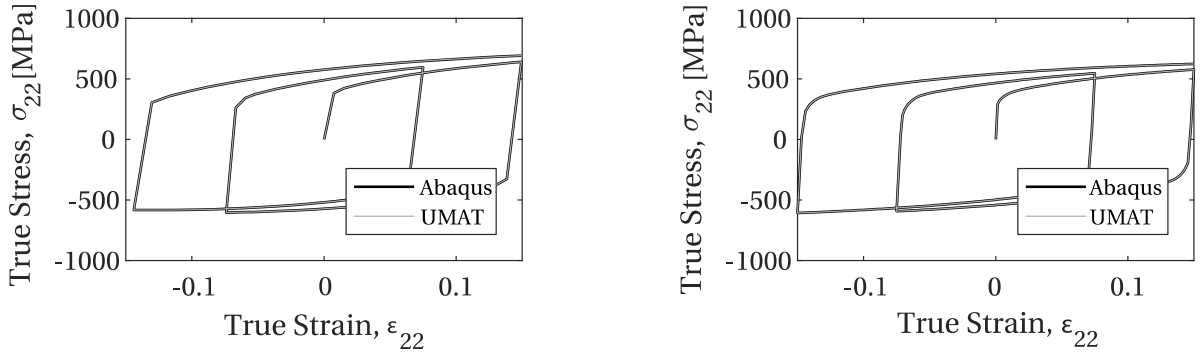

(a) Plane-stress *(b) Multiaxial*

Figure 2. Validation of the Abaqus UMAT for plane-stress and multiaxial stress states. The direct stress component in the "22" (i.e., yy) axis is shown in these figures.

Material model parameters

The original and updated Voce-Chaboche material models are both defined by multiple parameters. These parameters shall be chosen to closely replicate the material's stress-strain behavior regardless of the imposed load history. Inverse plasticity problems involving material parameter identification are challenging due to the nonlinear nature of this problem, and the non-uniqueness of the obtained model parameter set [20]. A gradient-based optimization method similar to that in de Castro e Sousa and Lignos [18] is used to find a set of parameters to fit the data. The details of this method are not discussed herein due to brevity, however later examples demonstrate the appropriateness of the chosen method to matching the steel's behavior under monotonic and cyclic loading.

Fundamental to the behavior of mild steels is that they exhibit strain hardening behavior. For this reason, constraints are integrated within the optimization method to ensure that the set of parameters always provides a hardening response. In other words, material softening is categorically excluded from the model response. The authors consider this constraint to be essential for the proper use of the rule expressed in Eq. (2).

Parameters for both the original and updated Voce-Chaboche models are provided in Table 1 for two backstresses. Calibrations with the same dataset show that two backstresses provide a reasonable compromise between efficiency and accuracy [18]. For both material models, the parameters are calibrated from the same set of coupons taken from a 25 mm thick plate of S355J2+N steel. This steel is equivalent to CAN/CSA G40.21 350 MPa and ASTM A992 Gr. 50 (nominal yield stress, f_y = 345 MPa) steels. The S355J2+N 25 mm dataset consists of 10 coupons from the same steel plate each tested with different cyclic loading protocols developed in a prior study [21]. Sample fittings from this dataset are shown in Figures 3a to 3d. The fit between the test data and both material models is noteworthy. The parameter D_∞ is set to 0.00 and a to 1.00 in the "Original" set of parameters to ignore the features of the updated model. Although there is a 20 % difference between the initial yield stresses of the two models, the overall fit between the two models is quite similar. Note that the difference in $\sigma_{y,0}$ is not clear in Figure 3a due to a relatively low number of data points in the measured stress-strain curve, however the difference is quite visible in Figure 3b and a zoom on the first load excursion of this test is shown in Figure 3c. As will be shown in the next section, the 20 % difference in initial yield stress has important implications for modeling steel wide-flange column instabilities.

Table 1. Parameters for the original and updated Voce-Chaboche material models with two backstresses for the S355J2+N 25 mm dataset. Original set of parameters from de Castro e Sousa and Lignos [18].

Model	E [GPa]	$\sigma_{y,0}$ [MPa]	Q_∞ [MPa]	b	D_∞ [MPa]	a	C_1 [MPa]	γ_1	C_2 [MPa]	γ_2
Original	191.52	265.29	104.44	11.63	0.00	1.00	12997.99	99.52	1560.41	7.35
Updated	185.97	332.18	120.48	8.14	93.15	261.75	21102.00	173.60	2300.60	10.42

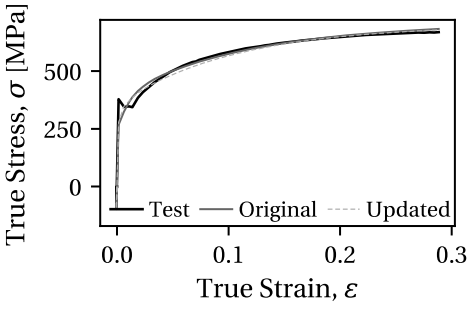

(a) Monotonic tensile load protocol

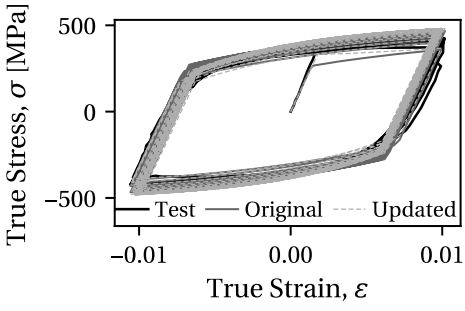

(b) Constant 2 % strain amplitude load protocol

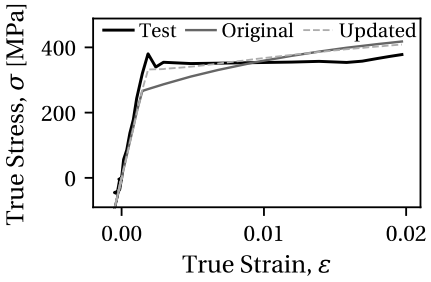

(c) Zoom on first load excursion

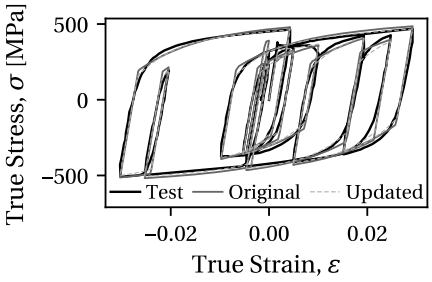

(d) Random strain load protocol

Figure 3. Selected tests to show the fitting of the S355J2+N 25 mm dataset for the parameters given in Table 1.

In addition to the increase in the initial yield stress, the yield plateau is more closely followed by the Updated model, as seen in Figure 3c. Therefore, the updated material model satisfies the two objectives of increasing the initial yield stress and better representing the plateau region. Observe that after the first loading cycle there is close agreement between the Original and Updated models. This is because the relatively large rate parameter a causes the additional term in Eq. (2) to saturate quickly, conceptually satisfying the notion that only the first loading excursion is affected. Finally, $Q_\infty > D_\infty$ in Table 1 for the updated material model; therefore, the gain in cyclic hardening is larger than the reduction in the yield surface after initial plastic loading in this case (see Figure 1b).

CASE STUDY

A case study is now presented to illustrate the dependence of instability modes on the choice of the material model. An HEB500 column with a length 7000 mm length and a constant axial load of $N = 0.2\ A\ \sigma_{y,0}$ (20 % axial load ratio) is chosen for this purpose. This column geometry is representative of first-story columns in steel moment-resisting frames. The column cross-section is similar to a W610X217 (W24X146) in North America. Relevant geometric properties of the column are summarized in Table 2. In this table, A is the cross-sectional area, h is the section depth (d CSA S16), b is the flange width (b_f CSA S16), t_w is the web thickness, t_f is the flange thickness, h_1 is the clear distance between flanges (h CSA S16), L_b is the column unbraced length, and i_z is the radius of gyration in the weak axis (r_y CSA S16). This column has relatively small web and flange slenderness ratios but a relatively large member slenderness ratio, L_b/i_z, making the column potentially susceptible to lateral-torsional buckling. However, it satisfies the Class 1 or highly ductile classification criteria for seismic design according to the Eurocode, CSA, and AISC provisions [22-24], respectively. Next the CFE models for this column are described, then the case study results are presented.

Column modeling guidelines

The HEB500 column is modeled in Abaqus 6.14 following the approach described by Elkady and Lignos [8]. The CFE model is illustrated schematically in Figure 4a. In brief, 4-node reduced integration shell elements (S4R) with enhanced hourglass control are used, a maximum mesh size of 30 mm is specified for these elements. Geometric imperfections corresponding to the first LTB and local buckling modes are imposed with amplitudes less than the fabrication tolerances specified by ASTM [25]. Fixed-fixed boundary conditions are assumed at each end of the column. A force is applied at the column top to simulate gravity loading, the magnitude of this force is always based on the "Updated" initial yield stress from Table 1. The AISC symmetric lateral loading protocol [24] is applied as a displacement boundary condition at the column top in-plane with the strong axis. A validation case is shown in Figure 4b for a W610X217 column ($h_1/t_w = 33.2, b/2t_f = 5.92, L_b/i_z = 51.0$) tested by Elkady and Lignos [2, 8] with similar boundary and loading conditions as the HEB500 case study. In this figure M_p is the plastic flexural capacity based on the measured material properties. Here, the relatively good match between test and simulated results indicates that the employed modeling approach can capture the initiation and progression of relevant geometric instabilities. Additionally, success by two of the authors in winning a recent international column blind analysis competition sponsored by the National Institute of Standards and Technology [26] suggests that the employed modeling procedure is reliable.

Two HEB500 column models are examined where the material response is modeled with the plane-stress implementation of the aforementioned UMAT. The "Original" column model is created following the guidelines with the "Original" material properties taken from Table 1, while the "Updated" column model is created following the exact same guidelines using the "Updated" material properties. Properties are taken from the 25 mm plate dataset to reasonably match the plate thickness of the flange and web thicknesses of the studied cross-section. We stress that the only difference between the two column models are the material parameters, and that these are calibrated based on the exact same material dataset.

Table 2. Geometric characteristics of an HEB500 column of 7000 mm length.

A [mm^2]	h [mm]	b [mm]	t_w [mm]	t_f [mm]	h_1/t_w	$b/2t_f$	L_b/i_z
23900	500	300	14.5	28	26.9	5.4	93.6

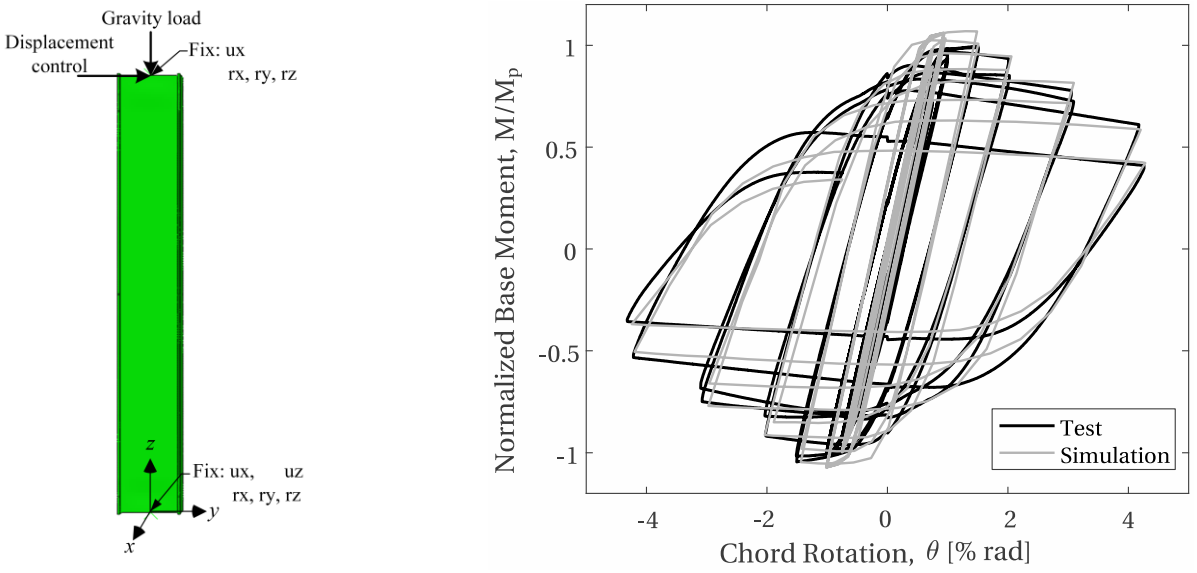

(a) Column model *(b) Validation case, W610X217 with 20 % axial load ratio*

Figure 4. Column model and validation case for the employed column modeling approach. Test and simulation data used with permission from Elkady and Lignos [2, 8].

Case study results

Key outcomes of the column case study are highlighted in this section. The base moment – chord rotation from both column models are plotted in Figure 5a. Observe that cyclic deterioration in flexural strength initiates at about 3 % chord rotation due to local buckling at the member ends. Despite the 20 % difference in $\sigma_{y,0}$ between the two material models, there is a nearly equivalent response between the column models with the original and the updated material models up to this point. The reason is that the Original set of material parameters provides a higher rate of initial hardening than the set parameters for the updated material model to compensate for the lower initial yield stress. However, after 3 % chord rotation a significant divergence is observed between the behavior of the column simulated with the Original and Updated models. The reason is that the two column models exhibit two substantially different instability modes, which are shown in Figure 5b and 5c, respectively. Note that at 5 % chord rotation the column employing the Original model has lost more than 50 % of its maximum flexural strength, while the same is not true for the column utilizing the Updated model. Therefore, if the member behavior at large deformations associated with structural collapse is of interest, the conclusions will be conflicting depending on the choice of the employed material model.

The case study presented in this section shows that the behavior of steel wide-flange columns may be sensitive to the steel material model choice. This sensitivity may not arise for all sets of geometric characteristics. The quantification of the range of cross-sections and column lengths requires a detailed sensitivity study, which is outside the scope of this paper. The shift in buckling modes shown in this case study leads to a fairly dramatic difference in the rate of strength and stiffness deterioration between the two examined instances. Differences in the rate of deterioration affects parameters of interest to structural engineers, such as the column's plastic deformation capacity and the extent of column axial shortening. The force redistribution within a structural system may also be significantly altered, which is a critical consideration for nonlinear collapse simulations.

Unfortunately, no comparison to component test data has been made thus far. This is because no full-scale column test exists where the material properties are fully known (i.e., several uniaxial or multiaxial coupons have been tested with different loading protocols for both the flange and web), and the geometric imperfections have been measured. Thus, a full-scale column test where the material properties, geometric imperfections, and residual stress measurements are accurately known should be carried out in the future for this purpose.

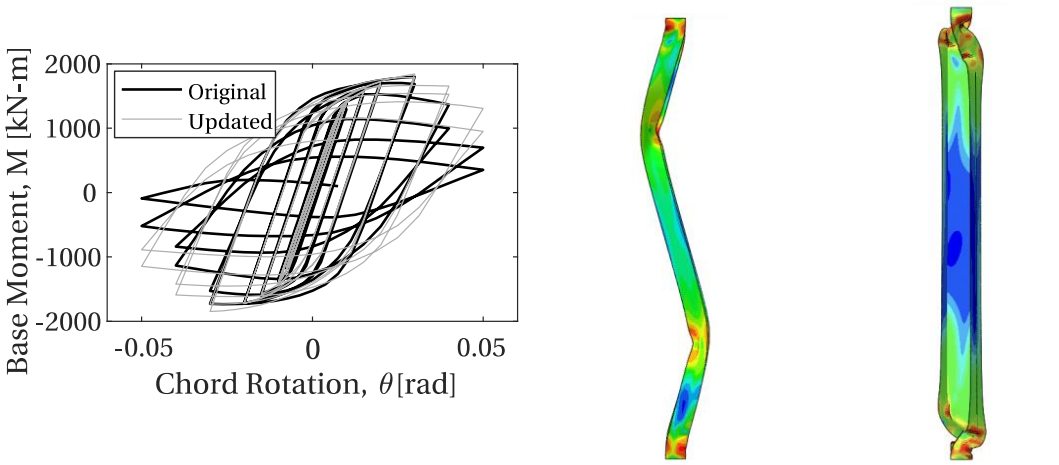

(a) Moment-rotation *(b) Original* *(c) Updated*

Figure 5. Moment – rotation and deformed shapes from the HEB500 column case study.

CONCLUSIONS

While previous finite element studies have taken for granted the material model used in continuum finite element (CFE) simulations involving buckling-induced softening of steel members, this study shows that the choice of material model can significantly affect the behavior of a class of steel wide-flange columns often used in today's seismic design of steel structures. This paper summarized deficiencies with a commonly utilized material model available in commercial CFE software. Updates to this material model are proposed to overcome a number of challenges. An illustrative case was also used where the behavior of a steel wide-flange column was shown to be sensitive to the choice of material model. The main findings are summarized as follows:

- The classic Voce-Chaboche metal plasticity model does not account for the discontinuous yielding phenomenon observed in mild steels. As such, the initial yield stress is naturally underestimated in parameter calibrations using cyclic loading protocols. An updated isotropic hardening rule is proposed to overcome this challenge. The uniaxial, plane-stress, and multiaxial implementations of this material model are implemented as UMATs for Abaqus (available at: https://resslab.epfl.ch/RESSLab-tools).
- The updated material model is shown to better estimate the initial yield stress when an optimization-based calibration method is used. There is a 20 % increase in the initial yield stress and plateauing is observed for the dataset of S355J2+N steel (equivalent to ASTM A992 Gr. 50) studied in this paper when the updated material model is used.
- An HEB500 column subjected to constant compressive axial load coupled with symmetric cyclic lateral load is simulated with both the original and updated material models. This case study demonstrates that steel wide-flange columns with large member slenderness (i.e., $L_b/i_z > 90$) that experience coupled local and lateral-torsional buckling may be sensitive to the choice of the metal plasticity material model.

Full-scale component tests where the material properties are known through several coupon tests, and the geometric imperfections are explicitly measured are required to further evaluate and validate the observations summarized in this paper.

ACKNOWLEDGMENTS

This study is based on work supported by École Polytechnique Fédérale de Lausanne (EPFL). The authors sincerely thank Dr. Ahmed Elkady for sharing his simulation and test data on one of the column tests he conducted in a prior study. Any opinions, findings, and conclusions or recommendations expressed in this paper are those of the authors and do not necessarily reflect the view of sponsors.

REFERENCES

[1] Cravero, J., Elkady, A., and Lignos, D. G. (2018). "Experimental Evaluation and Numerical Modeling of Wide-Flange Steel Columns Subjected to Constant and Variable Axial Load Couple with Lateral Drift Demands (Under Review)." *Journal of Structural Engineering*.

[2] Elkady, A., and Lignos, D. G. (2018a). "Full-Scale Testing of Deep Wide-Flange Steel Columns under Multiaxis Cyclic Loading: Loading Sequence, Boundary Effects, and Lateral Stability Bracing Force Demands." *Journal of Structural Engineering*, 144(2), 04017189.

[3] Newell, J. D., and Uang, C.-M. (2008). "Cyclic Behavior of Steel Wide-Flange Columns Subjected to Large Drift." *Journal of Structural Engineering*, 134(8).

[4] Ozkula, G., Harris, J., and Uang, C.-M. (2017). "Observations from Cyclic Tests on Deep, Wide-Flange Beam-Columns." *Engineering Journal*, 54(1), 45–59.

[5] Suzuki, Y., and Lignos, D. G. (2015). "Large Scale Collapse Experiments of Wide Flange Steel Beam-Columns." *8th International Conference on Behaviour of Steel Structures in Seismic Areas*, Shanghai, China.

[6] Suzuki, Y., and Lignos, D. G. (2017). "Collapse Behavior of Steel Columns as Part of Steel Frame Buildings: Experiments and Numerical Models." *16th World Conference on Earthquake Engineering (16WCEE)*, International Association of Earthquake Engineering, Santiago, Chile.

[7] Fogarty, J., and El-Tawil, S. (2015). "Collapse Resistance of Steel Columns under Combined Axial and Lateral Loading." *Journal of Structural Engineering*, 142(1).

[8] Elkady, A., and Lignos, D. G. (2018b). "Improved Seismic Design and Nonlinear Modeling Recommendations for Wide-Flange Steel Columns." *Journal of Structural Engineering*, 144(9), 04018162.

[9] Lignos, D. G., Hartloper, A. R., Elkady, A., Deierlein, G. G., and Hamburger, R. O. (2018). "Proposed Updates to the ASCE 41 Nonlinear Modeling Parameters for Wide-Flange Steel Columns in Support of Performance-based Seismic Engineering (Accepted for Publication)." *Journal of Structural Engineering*.

[10] Elkady, A., and Lignos, D. G. (2015). "Analytical investigation of the cyclic behavior and plastic hinge formation in deep wide-flange steel beam-columns." *Bulletin of Earthquake Engineering*, 13(4), 1097–1118.

[11] Voce, E. (1948). "The Relationship between Stress and Strain for Homogeneous Deformation." *Journal of the Institute of Metals*, 74, 537–562.

[12] Chaboche, J. L., Van, K. D., and Cordier, G. (1979). "Modelization of the strain memory effect on the cyclic hardening of 316 stainless steel." *Proceedings of the 5th International Conference on Structural Mechanics in Reactor Technology*, North-Holland Publishing Co., Berlin, Germany.

[13] Frederick, C. O., and Armstrong, P. J. (2007). "A mathematical representation of the multiaxial Bauschinger effect." *Materials at High Temperatures*, 24(1), 1–26.

[14] Cottrell, A. H., and Bilby, B. A. (1949). "Dislocation Theory of Yielding and Strain Ageing of Iron." *Proceedings of the Physical Society. Section A*, 62(1), 49.

[15] Hall, E. O. (1970). *Yield Point Phenomena in Metals and Alloys*. Plenum Press, New York, NY, USA.

[16] Lubliner, J. (2008). *Plasticity Theory*. Dover, New York, NY, USA.

[17] Abel, A., and Muir, H. (1972). "The Bauschinger effect and discontinuous yielding." *Philosophical Magazine*, 26(2), 489–504.

[18] de Castro e Sousa, A., and Lignos, D. G. (2018). *On the inverse problem of classic nonlinear plasticity models: An application to cyclically loaded structural steels*. Technical Report, Resilient Steel Structures Laboratory, École Polytechnique Fédérale de Lausanne (EPFL), Lausanne, Switzerland.

[19] Dassault Systèmes. (2014). *Abaqus Standard and Abaqus Documentation for version 6.14*. Dassault Systèmes Simulia Corp., Providence, RI, USA.

[20] Cooke, R. J., and Kanvinde, A. M. (2015). "Constitutive parameter calibration for structural steel: Non-uniqueness and loss of accuracy." *Journal of Constructional Steel Research*, 114, 394–404.

[21] Suzuki, Y., and Lignos, D. G. (2018). "Fiber-Based Model for Earthquake-Induced Collapse Simulation of Steel Frame Buildings." *Proceedings of the 11th National Conference on Earthquake Engineering*, Los Angeles, CA, USA, 11.

[22] EN. (2005). EN 1993-1-1: Eurocode 3: Design of steel structures - Part 1-1: General rules and rules for buildings. European Committee for Standardization, Brussels, Belgium.

[23] CSA. (2009). *CAN/CSA S16-09: Design of steel structures*. Canadian Standards Association, Mississauga, Canada.

[24] AISC. (2016). *Seismic provisions for structural steel buildings, ANSI/AISC 341-16*. American Institute of Steel Construction, Chicago, Illinois, United States.

[25] ASTM. (2016). Standard Specification for General Requirements for Rolled Structural Steel Bars, Plates, Shapes, and Sheet Piling. Standard, ASTM International, West Conshohocken, PA, United States.

[26] ATC. (2018). "ATC-106-1 Beam Column Blind Prediction Contest." <https://www.atcouncil.org/atc-106-blind-contest> (Feb. 15, 2018).